Average-atom models of line broadening in hot dense plasmas

J. Stein, D. Shalitin, and Akiva Ron
Racah Institute of Physics, The Hebrew University of Jerusalem, Jerusalem 91904, Israel
and Department of Physics and Astronomy, University of Pittsburgh, Pittsburgh, Pennsylvania 15260
(Received 1 February 1984; revised manuscript received 22 June 1984)

We present a method for estimating line broadening in the framework of a general average-atom model. This method is an extension of our previous work [Phys. Rev. A 29, 2789 (1984)]. It can reproduce the overall shapes of the "hilly features" present in spectra of hot dense plasmas in local thermodynamic equilibrium. Calculations are presented for a hafnium plasma, and the results are compared with experimental ones.

I. INTRODUCTION

The problem of the complex line spectrum of an atom in a hot dense plasma has been discussed in the past.[1-5] We present new modifications and extensions to these treatments. Our previous paper[5] (which we denote I) applied only to a Thomas-Fermi (TF) model. In Sec. II we describe our method which can be applied to any average-atom (AA) model. As in I this method starts with considering the fluctuations in occupation numbers, which in turn cause line broadening. We then proceed in either of two different modes: the "continuous mode" and the "discrete mode."

In the continuous mode we assume that the occupation numbers of electrons are continuously distributed around their nonintegral average values. These averages are the corrected AA values which are discussed in Sec. II A 1. From this point on we follow the method used in I. The lines between pairs of single-electron states which this procedure yields are broad and each of them represents a cluster of all lines between two single-electron levels. Then we discuss the similarities and differences of the two methods, namely, the TF model described in I and the present continuous mode. The discrete mode, which allows only integral occupation numbers, is very similar to the method which is described in the extensive review of Huebner.[4] We introduced it mainly for the purpose of checking our continuous-mode calculations.

In Sec. III we present results for a hafnium plasma at various densities and temperatures. We compare these new results with those of our previous TF method and with experiment.[6]

II. DESCRIPTION OF THE METHOD

Our starting point is the AA picture where we assume a fictitious atom having every atomic level populated by an average number (not necessarily integral) of electrons which agrees with the properties of the plasma (temperature, density, etc.). It gives an average spherically symmetric electrostatic potential $V^a(r)$ which can be considered as a zeroth-order approximation to the potential of the most probable configurations. We also have a set of single-electron wave functions $\psi_i(r)$, and to each corresponds an energy E_i^a (where i denotes a level). The wave functions and energy levels are obtained by solving the Schrödinger (or, as we do, the Dirac) equation. We also assume that the plasma is in local thermodynamic equilibrium (LTE) so that we have a temperature T, and a chemical potential (Fermi energy) μ, of the electrons. Then we can use the Fermi-Dirac distribution function to get the probability n_i that any particular state belonging to the ith level is occupied:

$$n_i=\frac{1}{e^{(E_i^a-\mu)/kT}+1} . \tag{1}$$

We assume that the populations of different states are uncorrelated, therefore the probability $P_i(N)$ for an atomic level i to be populated by N electrons is given by the binomial distribution:

$$P_i(N)=\begin{bmatrix} g_i \\ N \end{bmatrix} n_i^N (1-n_i)^{g_i-N} , \tag{2}$$

where g_i is the degeneracy of the level. The average population of level i is, therefore,

$$N_i^a=\sum_N NP_i(N)=n_i g_i . \tag{3}$$

Before proceeding to describe two modes of our method of line shift and broadening, we define the notation to be used in the following in order to distinguish different averaging schemes used in this section. Each average value has a superscript which identifies the scheme: a denotes average over all the atoms; e denotes average over all the electrons in a given level of all the atoms; h denotes average over all the holes in a given level of all the atoms; and t denotes average over all the transitions between two levels.

A. The continuous mode

1. Average level and line energies

The average-atom potential $V^a(r)$ is the average over all the atoms in the plasma of the atomic potential as seen by a test charge. This potential, in which the energy levels E_i^a and populations N_i^a are computed, is due to the aver-

 ©1985 The American Physical Society

age populations of the bound and free states.[7] When dealing with various types of transitions, like bound-free or bound-bound, different averages should be considered, yielding different populations—and hence different potentials and energy levels.

For the bound-free transitions we are interested in the probability $Q_i(N)$ that an electron in level i will have exactly $N-1$ neighbors in the same level of the same atom. The number of electrons having this property is naturally proportional to $NP_i(N)$ so that

$$\begin{aligned} Q_i(N) &= NP_i(N)/\sum_N NP_i(N) \\ &= NP_i(N)/N_i^a = NP_i(N)/n_i g_i \\ &= \binom{g_i-1}{N-1} n_i^{N-1}(1-n_i)^{(g_i-1)-(N-1)} . \end{aligned} \tag{4}$$

Under these conditions, the average number of electrons N_i^e as seen by an electron in level i (including itself) is

$$N_i^e = \sum_N NQ_i(N) = n_i(g_i-1)+1 . \tag{5}$$

[The average number of neighbors in level i is $n_i(g_i-1)$.] The average number of electrons in level $j \neq i$ as seen by an electron in level i is unchanged and equal to $n_j g_j$.

The potential, as seen by an electron in level i, is caused by its $n_i(g_i-1)$ neighbors, the $n_j g_j$ electrons in the other levels, and by the nucleus and the free electrons. It differs from the AA potential. To first order (ignoring exchange) this potential is

$$V_i^e(\vec{r}) = V^a(r) + \delta N_i^e v_i(\vec{r}) , \tag{6}$$

where $\delta N_i^e = -n_i$ and

$$v_i(\vec{r}) = \frac{1}{g_i}\sum_\epsilon \int |\psi_{i\epsilon}(\vec{r}')|^2 \frac{-e}{|\vec{r}-\vec{r}'|} d^3r' . \tag{7}$$

Here $\psi_{i\epsilon}$ are all the wave functions of the states of level i. As in I we approximate $v_i(\vec{r})$ by its spherical average $v_i(r)$, i.e., $1/|\vec{r}-\vec{r}'|$ is replaced by $1/\max(r,r')$, and Eq. (7) becomes

$$v_i(r) = \int_0^\infty \frac{-e}{\max(r,r')} |R_i(r')|^2 (r')^2 dr' , \tag{7'}$$

where R_i is the radial part of $\psi_{i\epsilon}$. The corrected average energy level becomes

$$E_i^e = E_i^a - n_i E_i^i , \tag{8}$$

where

$$E_i^j = -e\int_0^\infty |R_i(r)|^2 v_j(r) r^2 dr \tag{9}$$

is the first-order change in E_i due to addition of one electron in level j.

When considering transition probabilities from level i to level j, we are interested in the average populations of levels i and j as seen by the simultaneous pair of an electron in level i and a hole in level j. The average population of level i is given by Eq. (5). The average hole population in level j can be obtained in the same way Eq. (5) was obtained. Remembering that the probability of finding a hole in a state of level j is $1-n_j$, the average number of holes in this level, as seen by the hole (including itself), is

$$N_j^h = (1-n_j)(g_j-1)+1 . \tag{10}$$

The average population C_k^t of the core (i.e., all the other electrons) during a transition is therefore

$$\begin{aligned} C_k^t &= N_k^a = n_k g_k, \quad k \neq i,j \\ C_i^t &= N_i^e - 1 = n_i(g_i-1), \quad k=i \\ C_j^t &= g_j - N_j^h = n_j(g_j-1), \quad k=j . \end{aligned} \tag{11}$$

(Note that the core is the same for emission and absorption.) The correction to the energy levels will be

$$\begin{aligned} E_i^t &= E_i^a - n_i E_i^i - n_j E_i^j , \\ E_j^t &= E_j^a - n_i E_j^i - n_j E_j^j \end{aligned} \tag{12}$$

and the average transition energy

$$\begin{aligned} E_{ij}^t &= E_i^t - E_j^t \\ &= E_i^a - E_j^a - n_i(E_i^i - E_j^i) - n_j(E_i^j - E_j^j) . \end{aligned} \tag{13}$$

2. *Level and line broadening*

This is just a refinement of our treatment described in I. From Eq. (4) we get the mean square deviation $(\Delta N_{k,i}^e)^2$ of the population of the kth level as seen by an electron in the ith level:

$$\begin{aligned} (\Delta N_{k,i}^e)^2 &= \sum_N (N-N_k^e)^2 P_k(N) \\ &= g_k n_k(1-n_k), \quad k \neq i \\ (\Delta N_{i,i}^e)^2 &= \sum_N (N-N_i^e)^2 Q_i(N) \\ &= (g_i-1)n_i(1-n_i), \quad k=i . \end{aligned} \tag{14}$$

The change δE_i of the energy of level i due to the fluctuations δN_k in levels k is by Eq. (9)

$$\delta E_i = \sum_k \delta N_k E_i^k . \tag{15}$$

The average $[(\delta E_i)^2]^e$ over all the electrons in level i is

$$[(\delta E_i)^2]^e = \sum_{k,l} (\delta N_k \, \delta N_l)^e E_i^k E_i^l . \tag{16}$$

If the fluctuations are uncorrelated then

$$\begin{aligned} (\delta N_k \, \delta N_l)^e &= \delta_{kl}(\Delta N_{k,i}^e)^2 \\ &= \delta_{kl}(g_k - \delta_{ki}) n_k(1-n_k) , \end{aligned} \tag{17}$$

therefore, the average width ΔE_i^e of level i satisfies

$$\begin{aligned} (\Delta E_i^e)^2 &= [(\delta E_i^k)^2]^e = \sum_k (\Delta N_{k,i}^e)^2 (E_i^k)^2 \\ &= \sum_k n_k(1-n_k)(g_k - \delta_{ki})(E_i^k)^2 . \end{aligned} \tag{18}$$

In an analogous way we receive for the average transition width ΔE_{ij}^t,

$$(\Delta E_{ij}^t)^2=[(\delta E_{ij}^k)^2]^t=[(\delta E_i^k-\delta E_j^k)^2]^t$$
$$=\sum_k n_k(1-n_k)(g_k-\delta_{ki}-\delta_{kj})(E_i^k-E_j^k)^2 . \quad (19)$$

Equations (18) and (19) are the analogs of Eqs. (22) and (24) of I. ΔE_{ij}^t of Eq. (19) represents the width of the array distribution within the cluster of all transitions from level i to level j. As in I we assume that the shape of the cluster is Gaussian, but centered around E_{ij}^t rather than around E_{ij}^a.

Although derived by a similar method to the one used in I, and in spite of their similarity, the equations here and those analogous in I differ. There we used the whole available phase space whereas here we use only bound levels of relatively long lifetimes.

B. The discrete mode

The continuous mode, which has been described in Sec. II A has the advantage of simplicity. It depends, however, on a crucial assumption: the lines should merge to form the above-mentioned "hilly features." In order to estimate whether this assumption is fulfilled for the given temperature and density, we have to go beyond the single-particle model. Then we can estimate the amount of overlap between the lines and get a spectrum which has some "noise" and, therefore, is more similar to the experimental results.

In the discrete mode, which is similar to the one discussed in Ref. 4, Sec. III A, we treat the occupation numbers as integers. Therefore, instead of the continuous smearing of the lines we have each single-electron transition split into a cluster of lines, where each line represents an array of all the transitions between two configurations. By attributing a finite width to each line (array) we can then estimate the amount of overlap.

In order to split the single-electron lines we use first-order perturbation theory, i.e., Eqs. (6)—(9). We reduce the enormous number of configurations which is thus obtained by taking into account only those configurations having an occurrence probability which is not less than ϵ_p of that of the most probable one. Still we were left with a quite large number (hundreds of thousands for ϵ_p between 10^{-5} and 10^{-7}) of configurations and a larger number of lines.

The spectrum achieved this way consists of discrete lines. The emission intensity $I_{ij}^{\alpha\beta}$ from level i of configuration α to level j of configuration β is

$$I_{ij}^{\alpha\beta}=I_{ij}P(\alpha)N_i^\alpha\left[1-\frac{N_j^\alpha}{g_j}\right], \quad (20)$$

where I_{ij} is the single-electron emission intensity for one electron in level i to all states of level j (assuming that they are empty). At this stage each array of lines is represented by a single transition. There are various models for treating these arrays. We shall mention two of them.

In the model which we denote the "dense-array" model one assumes that the lines of an array merge together to form a broad line but the arrays themselves may be separate. The width of the line and a discussion of the physical conditions which are suitable for the application of this method are given by Bauche-Arnoult *et al.*[8] The other model, which we denote the "sparse-array" model, is far simpler. It assumes that each array has a given number, say K, of nonoverlapping lines, each having about the same intensity and width (e.g., Doppler width). Without increasing the overlap probability we can replace these K lines by a single one having K times the width of a single line. K is a small number, usually $1\lesssim K\lesssim 10$, and represents the typical number of strong lines in an array. This assumption is justified for the case of high-density high-temperature plasmas (although not too high). We used the latter model.

III. RESULTS AND DISCUSSION

We have applied the TF, the continuous mode, and the discrete mode to a hafnium ($z=72$) plasma. We present calculations for temperatures of 300 and 400 eV, and ion densities 5×10^{19} and 5×10^{20} ions/cm^3. Since the number of free electrons per atom was about 40—50, depending on the particular case considered, the electron densities were approximately 2×10^{21} and 2×10^{22} electrons/cm^3. We tried this range of temperatures and densities[9] in order to match the experimental data (see Fig. 1).[6] In our demonstration of the discrete mode we used the sparse-array model for broadening, and ignored all but Doppler broadening of the individual lines. The AA data were the same as in I, i.e., relativistic wave functions with nonrelativistic finite-temperature TF potential and Fermi energy.

The comparison between the TF and the continuous mode are shown in Figs. 2—5. The TF levels were shifted [by using Eq. (13) for the line center rather than $E_i^a-E_j^a$] to make the comparison easier. The energy shifts are always positive and are of the order of a few tens of eV.

In two graphs the TF "hills" are much broader than those of the continuous mode. This difference is due to the discrete nature of the quantum levels as opposed to the continuous nature of the TF phase space. In the cases considered here one can divide the energy levels into two groups: the upper levels $n\geq4$ are much higher than the Fermi energy. They are almost empty and the fluctua-

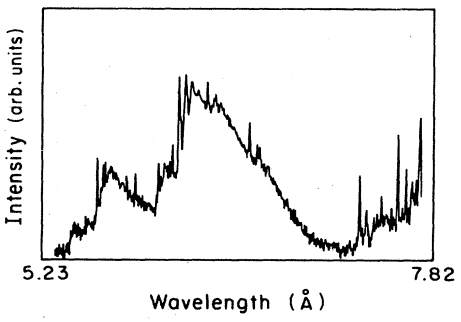

FIG. 1. The experimental spectrum of a hafnium plasma obtained by Zigler *et al.* (Ref. 6).

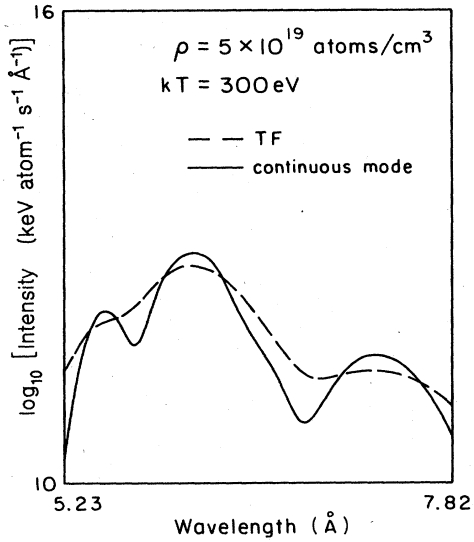

FIG. 2. The calculated emission spectrum of a hafnium plasma of density $\rho=5\times10^{19}$ atoms/cm^3 and temperature $kT=300$ eV according to the continuous mode and the TF model. The TF lines were shifted (see Sec. II A 1) so that the comparison is made easier.

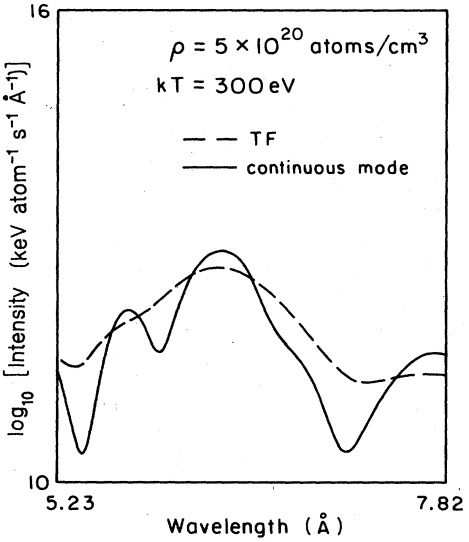

FIG. 4. Same as Fig. 2 but for $\rho=5\times10^{20}$ atoms/cm^3 and $kT=300$ eV.

tions of their populations are small. The lower levels $n\leq3$ are much lower than the Fermi energy, they are almost full, and, again, the fluctuations of their populations are small. In the TF model the energy "levels" are continuous and there are always some states near the Fermi level with large fluctuations. In Fig. 3, the Fermi energy is lower than in the other cases and is near to the $3d$ levels of the lower group. This causes large fluctuations in the populations of these levels and results in hills which are even slightly broader than the TF hills. The curves of the continuous mode in Figs. 2 and 4 are very similar to the experimental spectrum. The resemblance is naturally better than with the TF curves. A good fit to the experiment would be, for $\rho=5\times10^{19}$ atoms/cm^3 and temperature $kT\simeq280$ eV, or for $\rho=5\times10^{20}$ atoms/cm^3 and temperature $kT\simeq300$ eV. The central peak in Figs. 2—5 is due to the three $4f\rightarrow3d$ transitions, the right (long wave) peak is due to the three $4p\rightarrow3d$ transitions and the left peak (where shown) is due to the two $4d\rightarrow3p$ transitions. The central and left peaks have also some small contributions from $4s\rightarrow3p$ transitions.

The results of the discrete mode are shown in Fig. 6, for density 5×10^{19} atoms/cm^3 and temperature 300 eV. K, the number of lines per array, is 5. We changed the scale

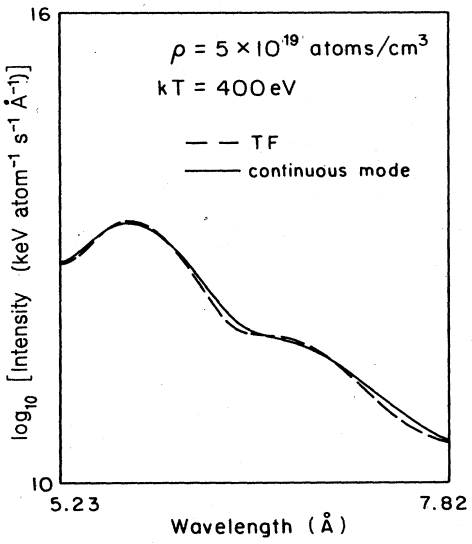

FIG. 3. Same as Fig. 2 but for $\rho=5\times10^{19}$ atoms/cm^3 and $kT=400$ eV.

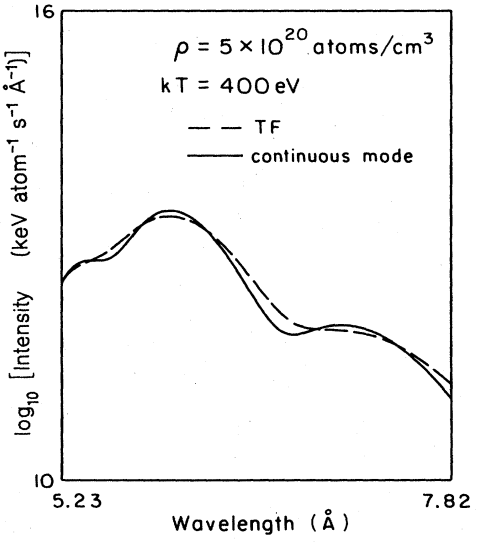

FIG. 5. Same as Fig. 2 but for $\rho=5\times10^{20}$ atoms/cm^3 and $kT=400$ eV.

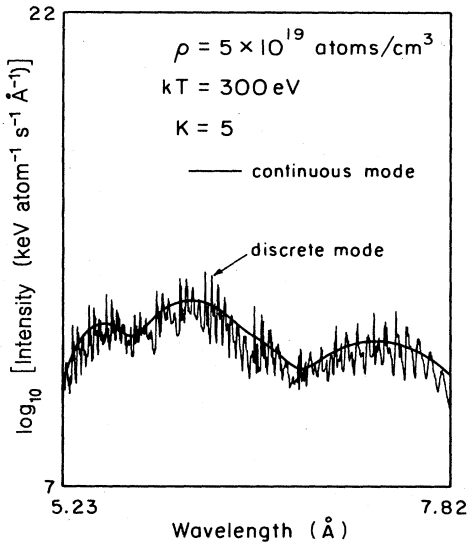

FIG. 6. Emission spectrum of a hafnium plasma at a temperature of 300 eV and density of 5×10^{19} atoms/cm^3 calculated according to the discrete mode (thin wiggly line) and the continuous mode (solid heavy line). Each line in the discrete spectrum has a Gaussian shape and a width which is $K=5$ times the Doppler width. The scale differs from that of the former figures in order to reveal the hills in the discrete spectrum.

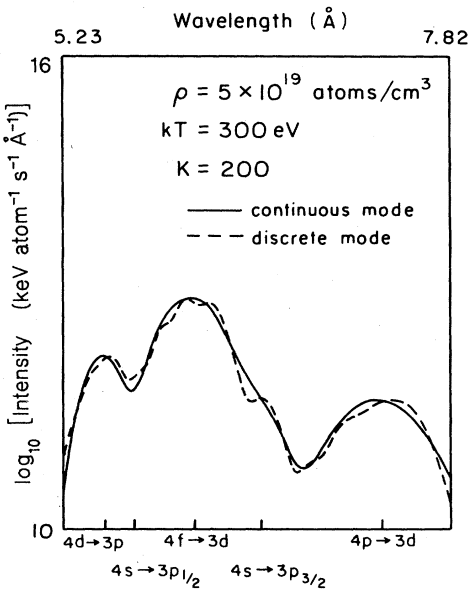

FIG. 7. Same as Fig. 6 but for $K=200$. Thus we compare the continuous mode with the averaged results of the discrete mode which assumed a width of 30—40 eV. The averaged-discrete-mode curve shows the two $4s\rightarrow3p$ transitions on both slopes of the main peak.

of this graph to reveal its overall shape. We tried also $K=2,10$ and the differences were hardly noticeable, so that we feel confident that the lines do merge.[10] In all cases the curve of the continuous model looks like a smooth average of the discrete mode. In Fig. 7 we compare the curve of the continuous mode with a curve of the discrete mode smoothed by setting $K=200$ (array width of 30—40 eV).

A very detailed comparison of the calculated and measured spectra is, of course, meaningless. The experimental measurements do not represent a homogeneous, LTE plasma with constant density and temperature. The scale of the experimental graph is not only arbitrary but not necessarily constant throughout the wavelength range. Nevertheless the resemblance is remarkable. It should be mentioned here that the temperature in our calculations was chosen, out of a range between 200 and 1000 eV, by mere comparison of shapes. Only after choosing these temperatures did we find out that the identified lines fit our hills very nicely. Since bulky shapes are easier to measure and identify then individual lines, this method might become an interesting diagnostic tool.

ACKNOWLEDGMENT

We wish to thank Professor R. H. Pratt for introducing us to this field and for his continuous encouragement.

[1]H. Mayer, Los Alamos Scientific Laboratory Report No. LA-647, 1948 (unpublished).

[2]A. N. Cox, in *Stars and Stellar Systems, Vol. 8: Stellar Structure,* edited by L. H. Aller and D. B. McLaughlin (University of Chicago, Chicago, 1965).

[3]T. R. Carson, D. F. Mayers, and D. W. N. Stibbs, Mon. Not. R. Astron. Soc. **140**, 483 (1968); T. R. Carson and H. M. Hollingsworth, *ibid.* **141**, 77 (1968).

[4]W. F. Huebner, Los Alamos National Laboratory Report No. LA-UR-81-2347, 1981 [in *Physics of the Sun* (Reidel, Dordrecht, in press)].

[5]D. Shalitin, J. Stein, and Akiva Ron, Phys. Rev. A **29**, 2789 (1984).

[6]A. Zigler, H. Zmora, N. Spector, M. Klapisch, J. L. Schwob, and A. Bar-Shalom, J. Opt. Soc. Am. **70**, 129 (1980).

[7]This assumption is not strictly valid in the case of TF potentials since the averages used deviate from the self-consistent values of the TF model. However, as was shown in the Appendix of I, these deviations are small.

[8]C. Bauche-Arnoult, J. Bauche, and M. Klapisch, Phys. Rev. A **20**, 2424 (1979); **25**, 2641 (1982).

[9]D. Salzmann (private communication).

[10]The merging could be improved by assuming Lorentzian shapes which occur in certain line-broadening mechanisms. However, it was unnecessary in our examples. We are grateful to Dr. W. F. Huebner and Dr. B. F. Rozsnyai for drawing our attention to this point.